RESEARCH ARTICLE

Figures and figure supplements

Testing the ion-current model for flagellar length sensing and IFT regulation

Hiroaki Ishikawa *et al*.

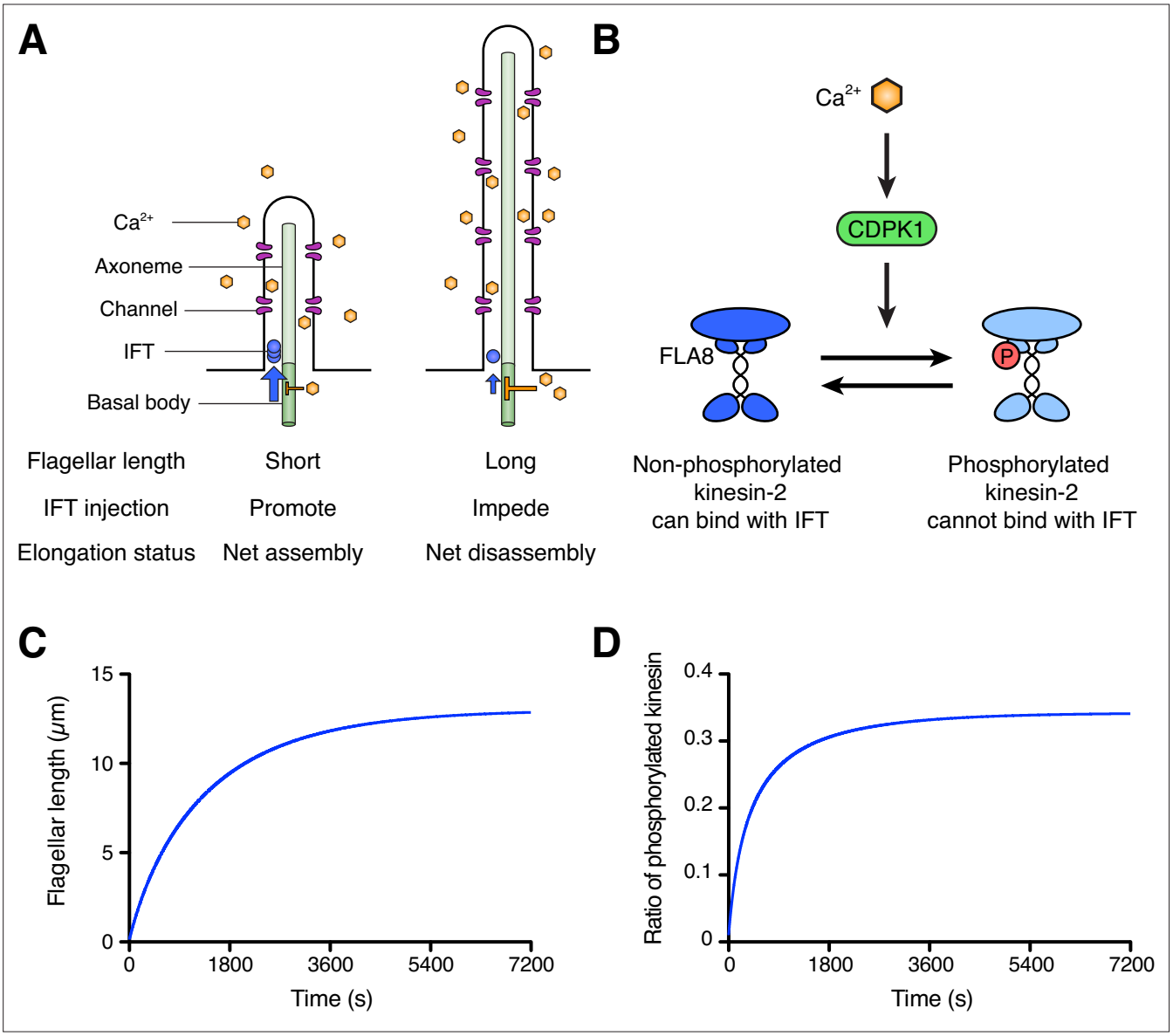

Figure 1. Schematic diagram and modeling of the ion-current model. (**A**) The ion-current model assumes the ion channels are uniformly distributed along the length of the flagellum, and Ca^{2+} ions entering the flagellum are proportional to the flagellar length. Flagellar Ca^{2+} is assumed to negatively regulate IFT injection into flagella to control the flagellar length. The longer flagellum can intake more ions, and these ions inhibit IFT injection such that the further assembly of flagella is suppressed. (**B**) The schema of kinesin-2 inactivation by Ca^{2+} and CDPK1 based on ***Liang et al., 2014***. In a Ca^{2+}-dependent manner, CDPK1 phosphorylates FLA8, a subunit of heterotrimeric kinesin-2. Phosphorylated kinesin-2 loses its IFT protein binding activity. (**C, D**) Simulated result of the ion-current model based on kinesin-2 phosphorylation by CDPK1 (***Liang et al., 2014***), as detailed in Materials and methods. Flagellar length (**C**) and the ratio of phosphorylated kinesin (**D**) were plotted against time.

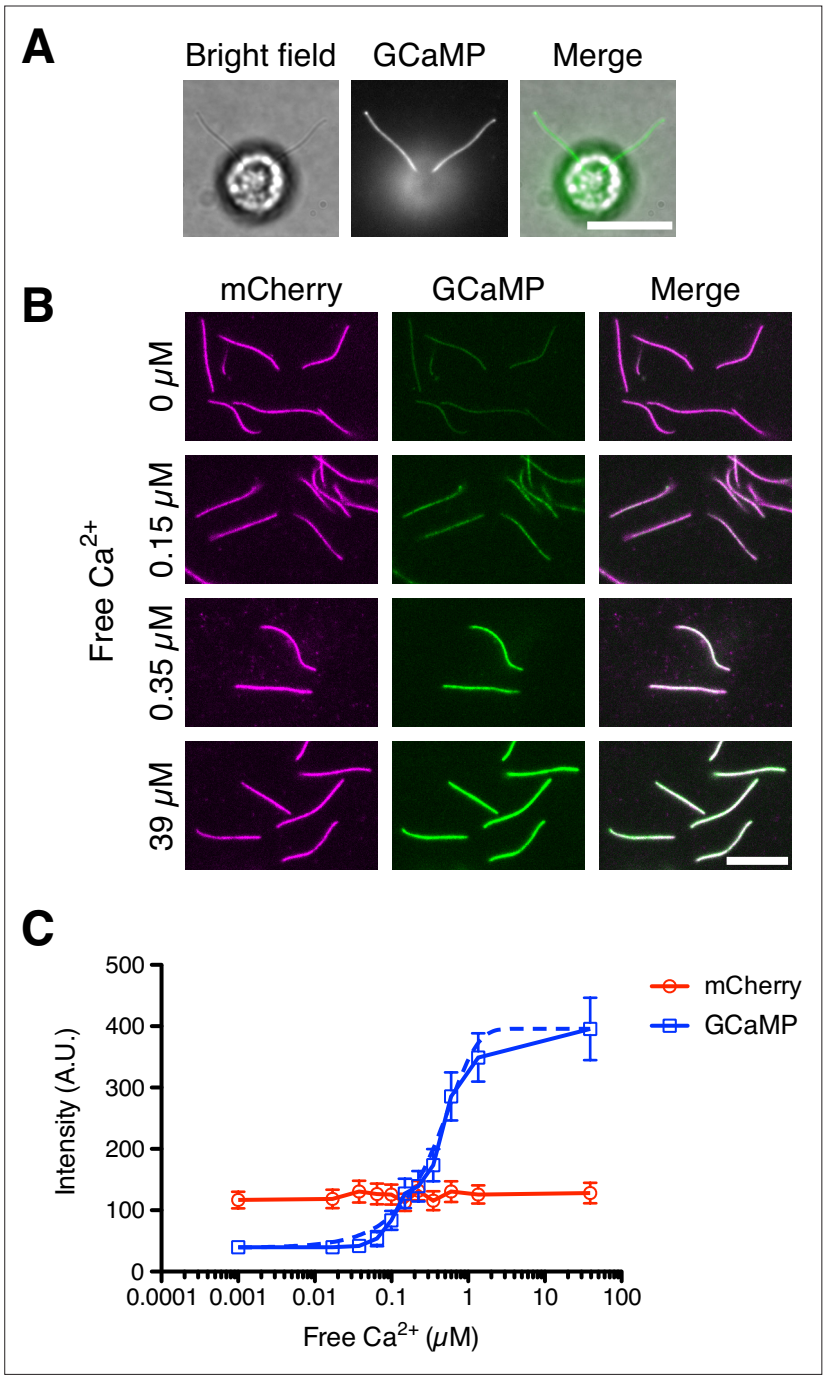

Figure 2. DRC4-GCaMP quantitatively detects free Ca^{2+}. (**A**) Bright-field and fluorescent images of DRC4-GCaMP cells. DRC4-GCaMP localizes to the entire length of flagella. Scale bar: 10 μm. (**B**) Fluorescent images of isolated DRC4-mCherry-GCaMP axonemes. Axonemes were isolated from DRC4-mCherry-GCaMP cells and were treated with various concentration of free Ca^{2+}. GCaMP intensity increased as free Ca^{2+} concentration increased. Scale bar: 10 μm. (**C**) Semilogarithmic plot of GCaMP and mCherry intensities. GCaMP and mCherry intensities were measured and plotted with mean ± SD. Thirteen axonemes were analyzed for each Ca^{2+} concentration. The blue dashed line shows the equation of a sigmoidal curve which is calculated from the data.

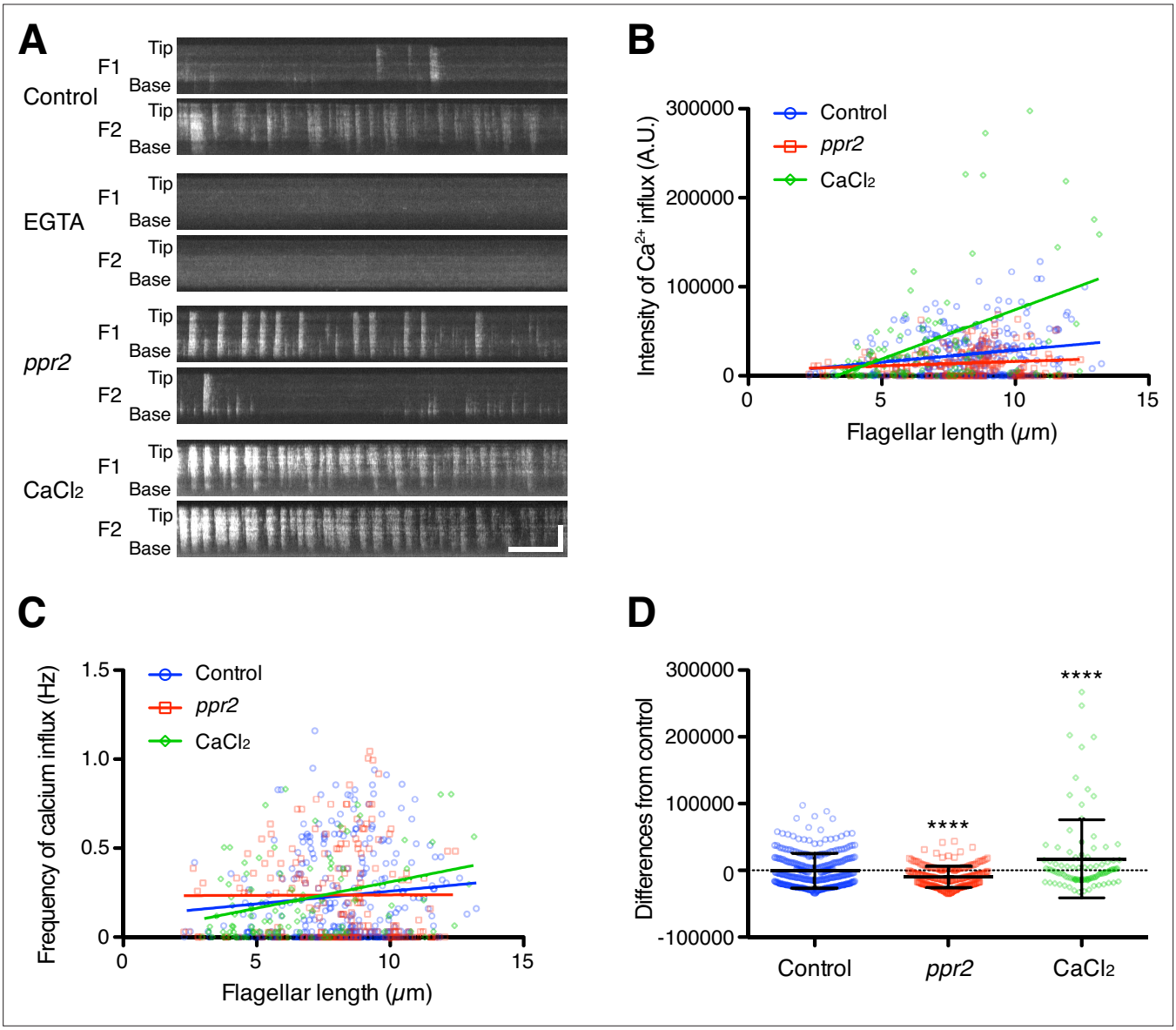

Figure 3. Quantification of Ca2 +influx as a function of flagellar length. (**A**) Representative DRC4-GCaMP kymographs of *Chlamydomonas* flagella in control (*pf2* DRC4-GCaMP), 1 mM EGTA-treated (*pf2* DRC4-GCaMP), *ppr2* mutant (*pf2 ppr2* DRC4-GCaMP), and 1 mM $CaCl_2$-treated (*pf2* DRC4-GCaMP) cells. These kymographs were assembled from ***Videos 1–4***. Horizontal bar: 5 s; vertical bar: 5 μm. (**B**) The intensity of Ca^{2+} influx into flagella was calculated from kymographs and plotted against flagellar length. Different lengths of flagella were obtained by imaging flagella during regeneration. Control (blue circles, n=272, Pearson correlation coefficient ρ =0.21, and coefficient of determination r^2=0.04), the *ppr2* mutant (red squares, n=182, ρ =0.14, and r^2=0.02), and 1 mM $CaCl_2$-treated cells (green diamonds, n=96, ρ =0.46, and r^2=0.21). (**C**) The frequency of Ca^{2+} influx was plotted against flagellar length. No obvious correlation was detected in either the control (blue circles, ρ =0.11, and r^2=0.01) or the *ppr2* mutant (red squares, ρ =0.004, and r^2=1.85 × 10^{-5}). However, the frequency of Ca^{2+} influx in 1 mM $CaCl_2$ treated cells was correlated with flagellar length (green diamonds, ρ =0.33, and r^2=0.11). (**D**) The mean differences of Ca^{2+} influx intensity from the control regression line. Data were plotted as scatter dot plots with mean ± SD. Statistical significance was determined by an unpaired two-tailed t test against the control (**** p<0.0001).

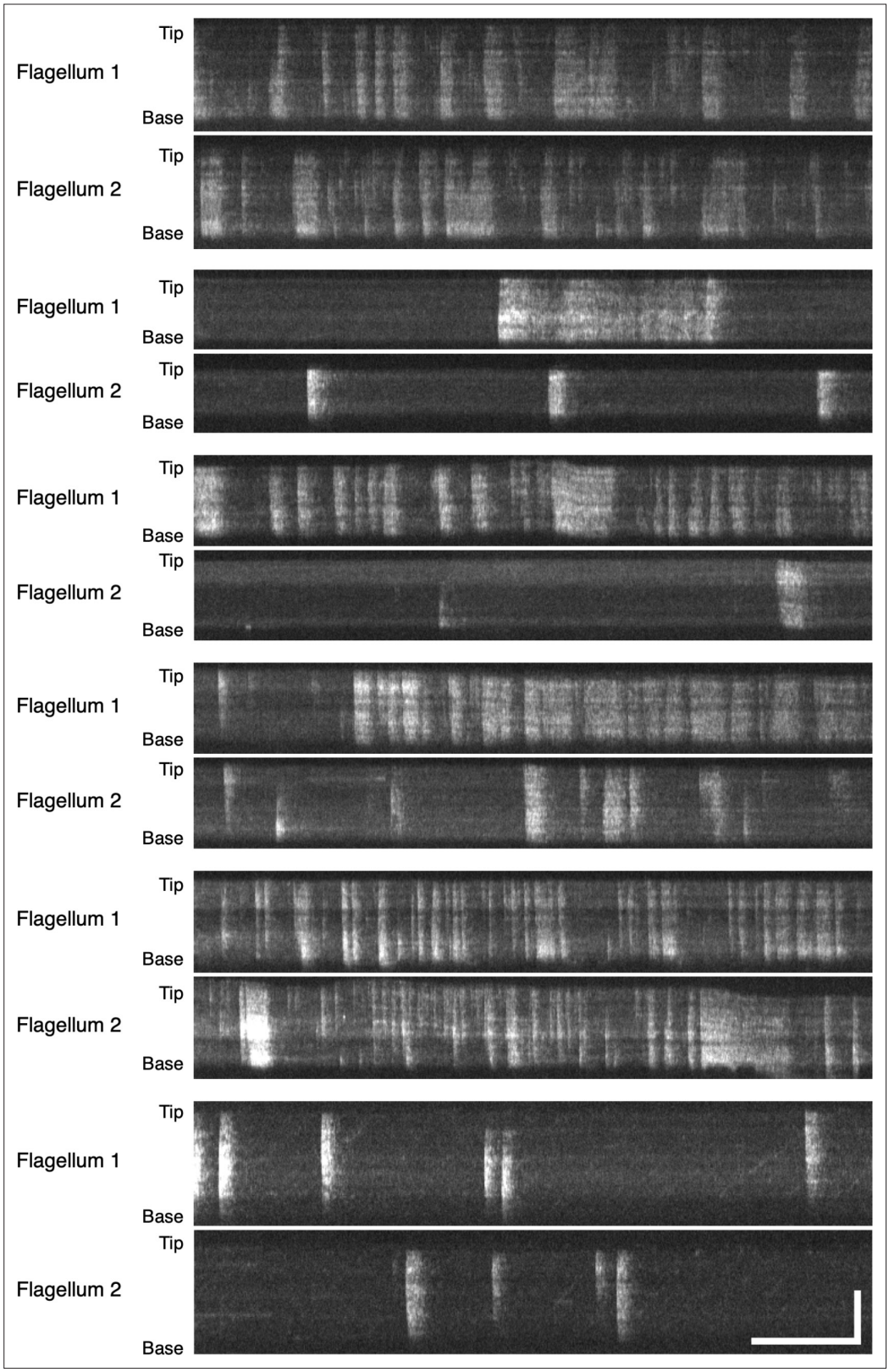

Figure 3—figure supplement 1. Example DRC4-GCaMP kymographs of *Chlamydomonas* flagella (control, *pf2* DRC4-GCaMP). The pair of Flagellum 1 and Flagellum 2 are flagella from the same cells. The pattern of Ca^{2+} influx events varied from flagellum to flagellum and from time to time. Horizontal bar: 5 s; vertical bar: 5 μm.

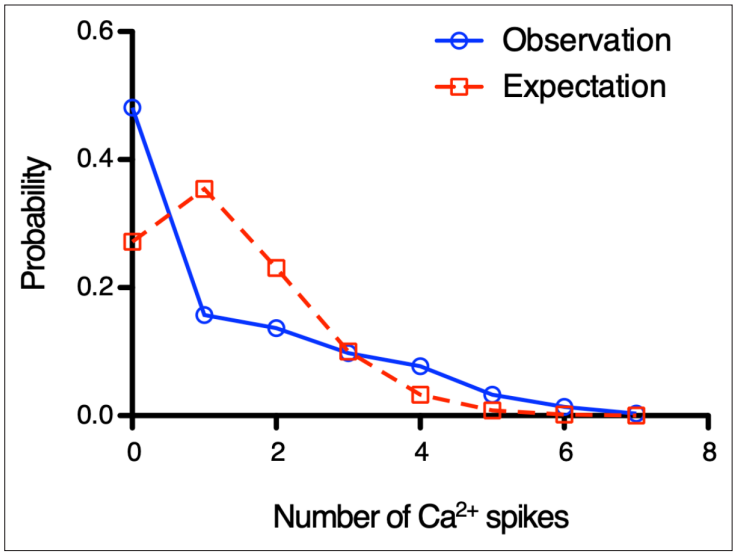

Figure 3—figure supplement 2. Individual Ca^{2+} influx events are not independent. Histogram shows Ca^{2+} spikes distribution every 5 s. Blue line shows the DRC4-GCaMP (control) data from ***Figure 3***. Red dashed line shows calculated data to fit with Poisson distribution. Blue line does not fit with red line (Chi-square goodness-of-fit test, $p<0.0001$). Similar results were obtained at other time intervals.

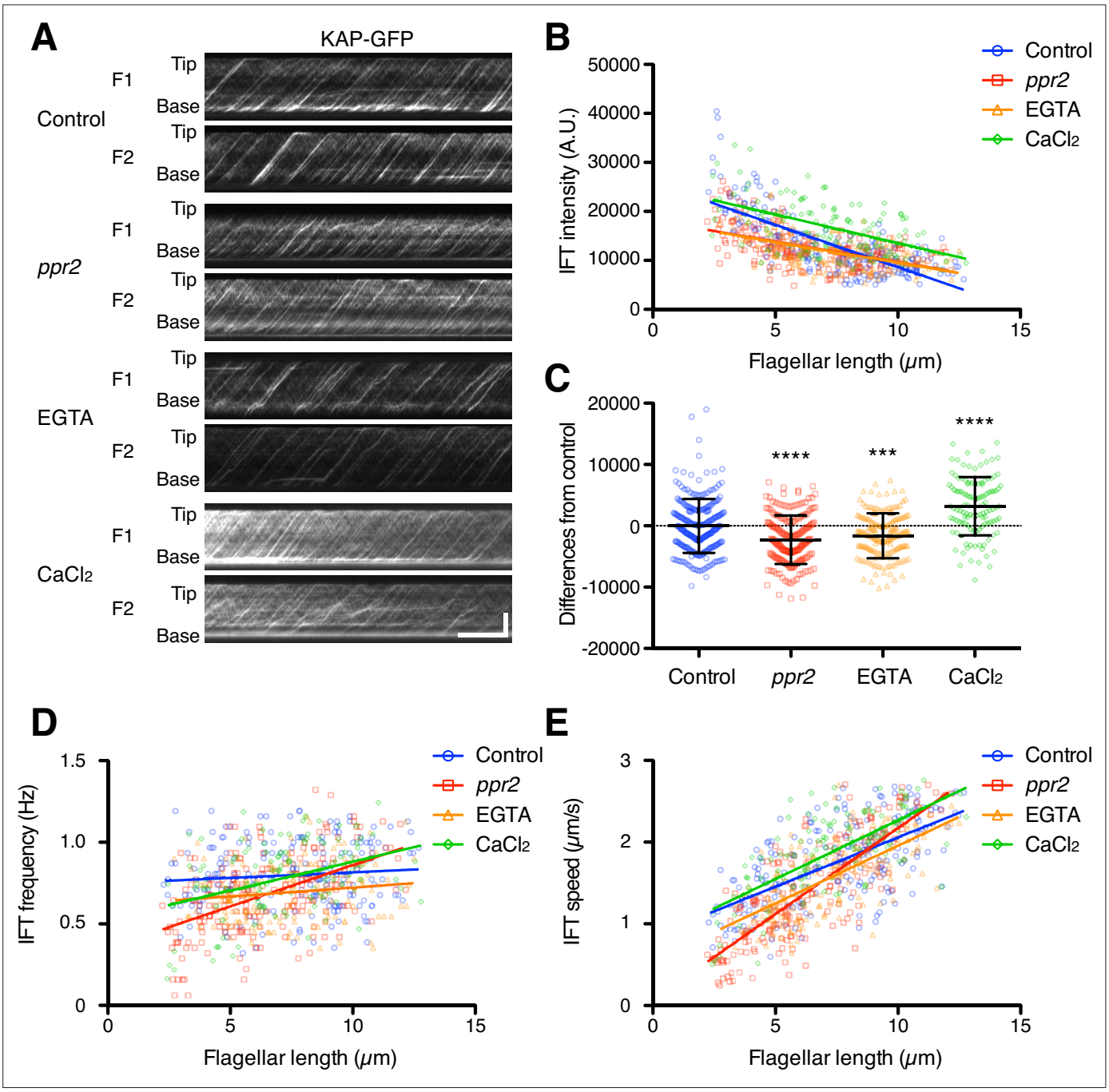

Figure 4. Quantification of IFT injection as a function of flagellar length. (**A**) Representative KAP-GFP kymographs of *Chlamydomonas* flagella in control (*fla3* KAP-GFP), *ppr2* mutant (*fla3 ppr2* KAP-GFP), 1 mM EGTA-treated (*fla3* KAP-GFP), and 1 mM $CaCl_2$-treated (*fla3* KAP-GFP) cells. These kymographs were assembled from ***Videos 5–8***. Horizontal bar: 5 s; vertical bar: 5 μm. (**B**) The mean KAP-GFP intensity of each flagellum was calculated from kymographs and plotted against flagellar length. Control (blue circles, n=220, ρ =–0.72, and r^2=0.51), *ppr2* (red squares, n=192, ρ =–0.52, and r^2=0.27), EGTA (orange triangles, n=162, ρ =–0.53, and r^2=0.28), and $CaCl_2$ (green diamonds, n=116, ρ =–0.52, and r^2=0.27). (**C**) The mean difference of IFT intensity from the control regression line. Data were plotted as scatter dot plot with mean ± SD. Statistical significance was determined by an unpaired two-tailed t test against the control (*** p<0.001; **** p<0.0001). (**D**) The frequency of KAP-GFP was plotted against flagellar length. Control (blue circles, ρ =0.17, and r^2=0.03), *ppr2* (red squares, ρ =0.51, and r^2=0.26), EGTA (orange triangles, ρ =0.14, and r^2=0.02), and $CaCl_2$ (green diamonds, ρ =0.38, and r^2=0.15). (**E**) The velocity of KAP-GFP was plotted against flagellar length. Control (blue circles, ρ =0.64, and r^2=0.41), *ppr2* (red squares, ρ =0.81, and r^2=0.64), EGTA (orange triangles, ρ =0.69, and r^2=0.47), and $CaCl_2$ (green diamonds, ρ =0.69, and r^2=0.48).

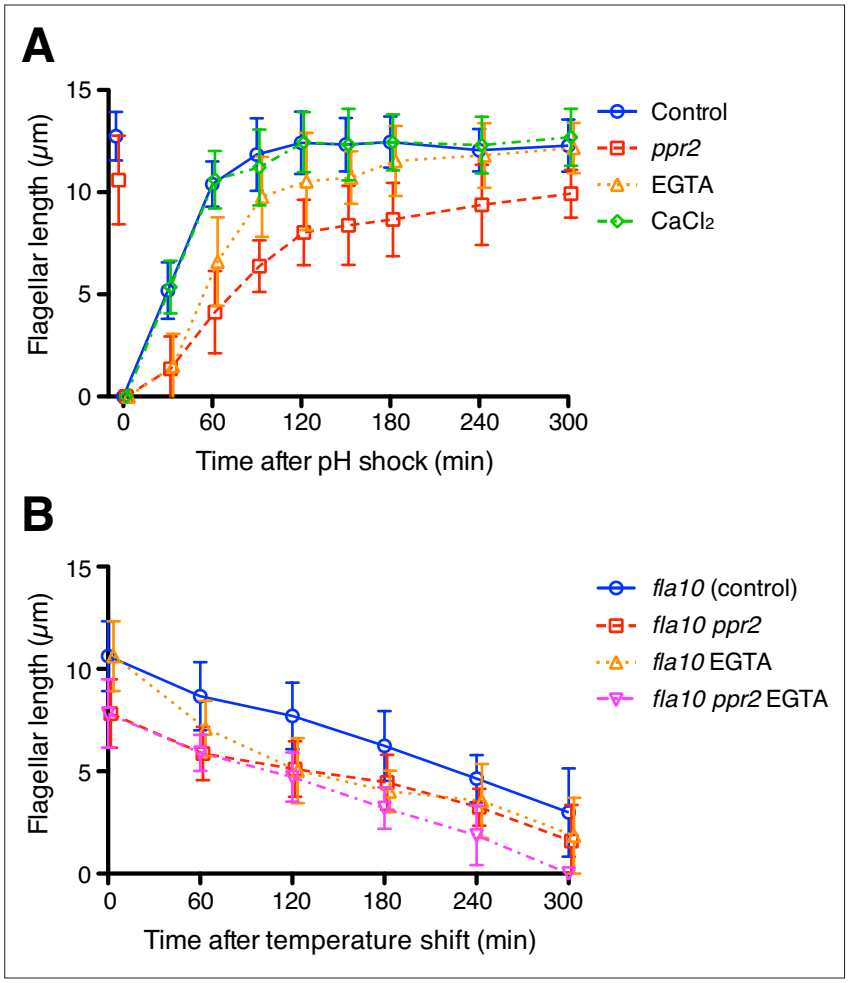

Figure 5. The kinetics of flagellar regeneration and disassembly. (**A**) Flagella were removed by the pH shock method. Mean flagellar length of control (wild-type CC-125, blue circles), *ppr2* mutant (red squares), 1 mM EGTA-treated (orange triangles), and 1 mM $CaCl_2$-treated (green diamonds) cells was plotted against time after pH shock. (**B**) The *fla10* mutant strains were transferred to the restrictive temperature (33 °C). Mean flagellar length of control (*fla10*, blue circles), *fla10 ppr2* mutant (red squares), 1 mM EGTA-treated *fla10* (orange triangles), and 1 mM EGTA-treated *fla10 ppr2* (magenta inverted triangles) cells was plotted against time after temperature shift. Twenty biflagellated cells were measured per strain and time point. Data were plotted with mean ± SD.

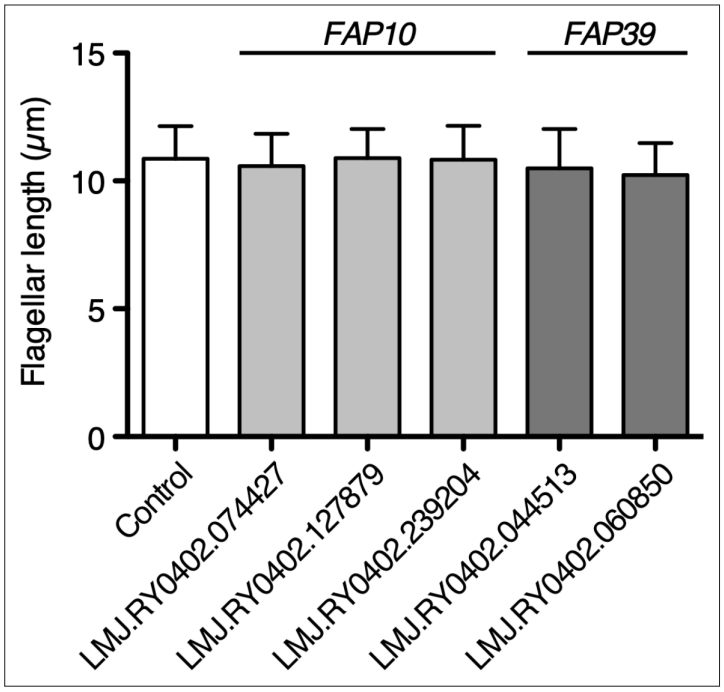

Figure 5—figure supplement 1. Flagellar length of potential flagellar calcium pump mutant cells. Potential mutant strains of FAP10 and FAP39 were obtained from the CLiP library. The control cell is the background strain of the library, CMJ030 (CC-4533 cw15 mt-). These mutations were identified from the CLiP library database and not independently verified. Twenty-five biflagellated cells were measured per strain. Data were plotted with mean ± SD. All mutant strains showed no significant differences in flagellar length from the control. Statistical significance was determined by an unpaired two-tailed t test against the control.

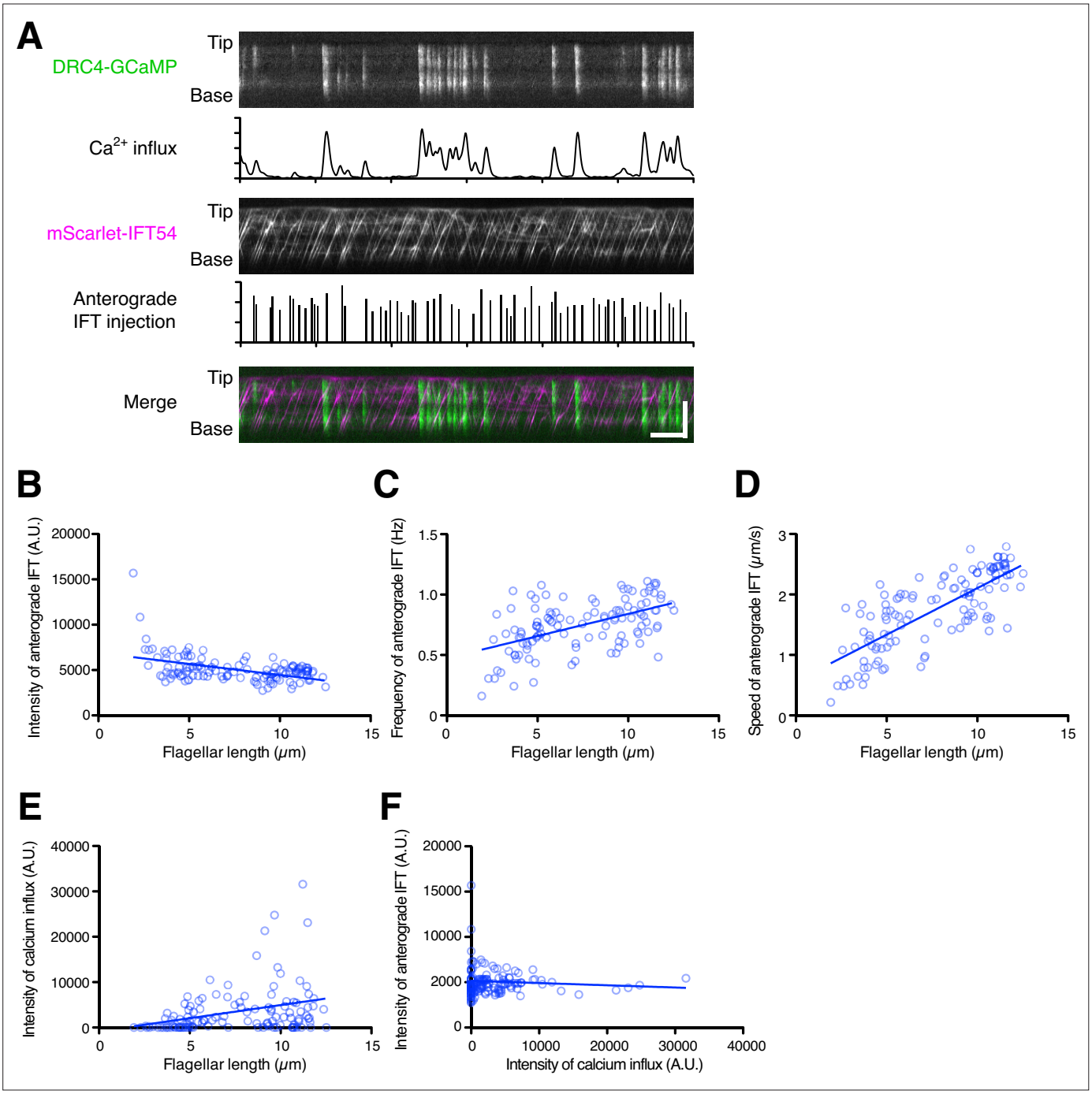

Figure 6. Dual-channel imaging of DRC4-GCaMP and mScarlet-IFT54. (**A**) Representative kymographs and quantified data. The DRC4-GCaMP kymograph (top) was generated from ***Video 9***. Quantified intensity of Ca^{2+} influx is shown at the bottom of the kymograph. The mScarlet-IFT54 kymograph (middle) was generated from ***Video 9***. Quantified anterograde IFT injection is shown at the bottom of the kymograph. The merged kymograph (bottom) of DRC4-GCaMP (green) and mScarlet-IFT54 (magenta). Horizontal bar: 5 s; vertical bar: 5 μm. (**B**) The mScarlet-IFT54 intensity of each flagellum was calculated from kymographs and plotted against flagellar length (n=116, and Pearson correlation coefficient ρ =–0.47). Non-linear regression is indicated by a solid line (r^2=0.21). (**C**) The frequency of anterograde IFT was plotted against flagellar length (ρ =0.53 and r^2=0.28). (**D**) The velocity of anterograde IFT was plotted against flagellar length (ρ =0.76 and r^2=0.58). (**E**) The intensity of Ca^{2+} influx into flagella was calculated from kymographs and plotted against flagellar length (ρ =0.33 and r^2=0.11). (**F**) The mean mScarlet-IFT54 intensity was plotted against the intensity of Ca^{2+} influx (ρ =–0.08 and r^2=0.007).

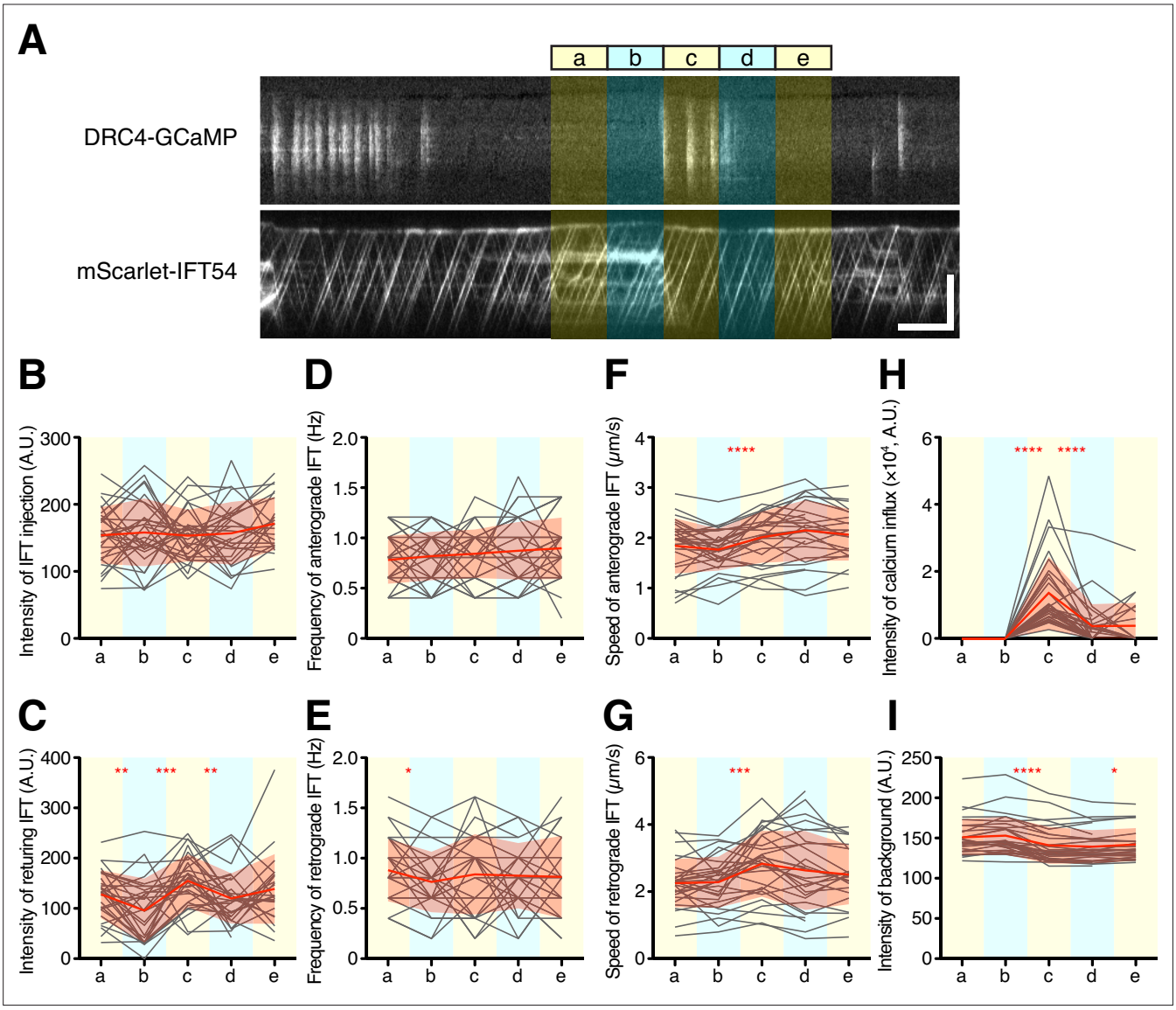

Figure 7. Quantification of IFT behavior after Ca^{2+} influx. (**A**) Overview of the short-time analysis of IFT behavior after a burst of Ca^{2+} influx using dual-channel imaging. Analyzed areas were colored on the representative kymographs of DRC4-GCaMP and mScarlet-IFT54. Intervals of each area are 5 s. Bursts of Ca^{2+} influx were selected where no previous Ca^{2+} influx was observed for more than 10 s before the Ca^{2+} influx. The 'c' area was set at the start of the burst of Ca^{2+} influx. The areas 'a' and 'b' were set to 10 s and 5 s before the burst of Ca^{2+} influx at the 'c' area. The areas 'd' and 'e' were set to 5 s and 10 s after the start of the Ca^{2+} influx, respectively. Horizontal bar: 5 s; vertical bar: 5 μm. (**B–G**) IFT behaviors before and after the burst of Ca^{2+} influx were plotted against each area (n=29). Gray lines show each analysis, and red lines and area show the mean and SD, respectively. (**B**) The intensity of IFT injection. (**C**) The intensity of returning IFT. (**D**) The frequency of anterograde IFT. (**E**) The frequency of retrograde IFT. (**F**) The speed of anterograde IFT. (**G**) The speed of anterograde IFT. (**H**) The sum of the Ca^{2+} influx before and after the burst of Ca^{2+} influx. (**I**) The background intensity of mScarlet-IFT54. Statistical significance between neighboring areas was determined by a paired two-tailed t test (* $p<0.05$; ** $p<0.01$; *** $p<0.001$; **** $p<0.0001$).

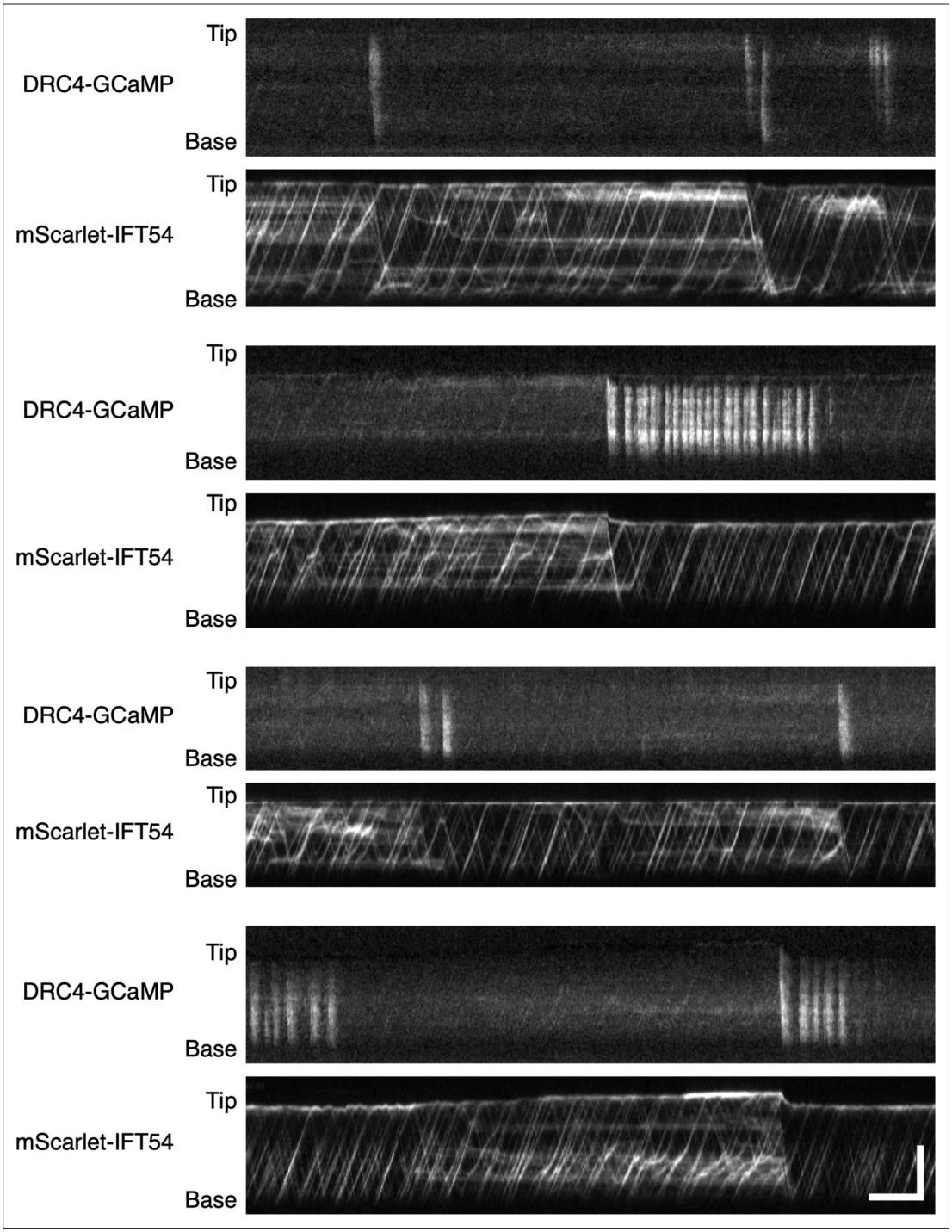

Figure 7—figure supplement 1. Additional examples of stalled IFT release by Ca^{2+} influx. Kymographs of DRC4-GCaMP and mScarlet-IFT54 were from four different flagella. mScarlet-IFT54 was paused and accumulated when Ca^{2+} influx was not observed for a long-time. These examples confirm that Ca^{2+} influx can clear paused IFT for flagella. Horizontal bar: 5 s; vertical bar: 5 μm.